Theofanis Strouboulis; Realino Hidajat
Partition of unity method for Helmholtz equation: q-convergence for plane-wave and wave-band local bases

PARTITION OF UNITY METHOD FOR HELMHOLTZ
EQUATION: q-CONVERGENCE FOR PLANE-WAVE
AND WAVE-BAND LOCAL BASES[1]

Theofanis Strouboulis, Realino Hidajat, College Station

Abstract. In this paper we study the q-version of the Partition of Unity Method for the Helmholtz equation. The method is obtained by employing the standard bilinear finite element basis on a mesh of quadrilaterals discretizing the domain as the Partition of Unity used to paste together local bases of special wave-functions employed at the mesh vertices. The main topic of the paper is the comparison of the performance of the method for two choices of local basis functions, namely a) plane-waves, and b) wave-bands. We establish the q-convergence of the method for the class of analytical solutions, with q denoting the number of plane-waves or wave-bands employed at each vertex, for which we get better than exponential convergence for sufficiently small h, the mesh-size of the employed mesh. We also discuss the *a-posteriori* estimation for any solution quantity of interest and the problem of quadrature for all integrals employed. The goal of the paper is to stimulate theoretical development which could explain various numerical features. A main open question is the analysis of the pollution and its disappearance as function of h and q.

Keywords: Partition of Unity Method (PUM), Helmholtz equation, exponential convergence, extrapolation, pollution due to wave-number

MSC 2000: 65J10

1. Introduction

The Partition of Unity Method (PUM) which was introduced in [1]–[5] is now used in many engineering computations. One of its many features is the possibility of employing special local basis functions defined on the supports of the partition of unity functions. Typically the PUM is combined with the classical FEM; see,

e.g., the Generalized FEM [6]–[10], and the extended FEM [11]. In this paper we will apply the (pure) PUM (i.e. the method obtained by pasting only basis functions defined over the supports of the partition of unity functions) for solving the Helmholtz problem given below in (2)–(3) with $f = 0$. We will choose the space of local basis functions to be the span of a set of functions which identically satisfy the homogeneous Helmholtz equation, $\Delta u + k^2 u = 0$. The main problem is the selection of the local basis functions. We must consider:

1. The approximation properties of the chosen set, more precisely
   (a) its completeness;
   (b) the estimate of the error in the best approximation.
2. The stability (inf-sup) of PUM.

In [5] and [2] these problems were addressed for two kinds of special functions, namely a) plane-waves, b) Bessel functions of the first kind arising from the theory of Vekua. The Fourier transform of the functions on $\mathbb{R}^2$ which satisfy the homogeneous Helmholtz equation (2a) has its support on the circle $\xi_1^2 + \xi_2^2 = k^2$; for example the plane-waves are images of Dirac functions located on the circle.

The purpose of this paper is to compare the performance of the PUM for the Helmholtz problem using two types of basis functions, namely

1. the plane-waves—which are images of Dirac functions on the circle,
2. the wave-bands—which are images of piecewise constant functions on the circle.

Let us note that the full theory for the wave-bands is not available. The numerical results presented here are employed to stimulate the important question of how to understand the behavior and properties of the PUM for the Helmholtz problem for each particular choice of the basis functions.

The local character of the solution of the Helmholtz problem (2) is different in the interior of the domain and in the neighbourhood of the boundary where the solution can also have "evanescent" character. Here we deal with the problem in the interior where the solution can be assumed to be analytic.

Since the initial works [2], [5] on the PUM for the Helmholtz, the method was further developed by Bettess, Laghrouche and their co-workers [12]–[16], by Ortiz and Sanchez [17] and Ortiz [18]; additional references may be found in these papers. Other methods with similar ingredients are the Discontinuous Enrichment Method of Farhat and co-workers [19], [20] which also employs local bases of plane waves using a Discontinuous Galerkin formulation with Lagrange Multipliers, and the Variational Theory of Complex Rays of Ladevèze, Rouch and co-workers [21]–[23] which uses local bases of wave-bands and a new mixed variational formulation of the Discontinuous Galerkin type.

Stability of the PUM for the Helmholtz can be analyzed by employing the pollution ratio

(1)
$$\pi_S(u) = \frac{\|\nabla(u - u_{\text{PUM}})\|_{L^2(\Omega)}}{\inf\limits_{\chi \in S} \|\nabla(u - \chi)\|_{L^2(\Omega)}}$$

where u is the exact solution, u_{PUM} is the PUM solution from the PUM space S. The ratio $\pi_S(u)$ compares the norm of the error in u_{PUM} versus the corresponding norm of the error in the best approximation for the PUM space S and the exact solution u; when $\pi_S(u)$ is close to one we can say that the pollution is negligible.

The pollution is a very important feature of numerical solution of the Helmholtz problem; it is a shift in the Galerkin solution due to numerical dispersion and it was addressed in [24]–[27]. The pollution is also related to the inf-sup condition which was proved in [5] under the condition $(1 + k^2)h \leqslant \mathscr{C}$. Another goal of the paper is to tackle numerically, as function of the mesh-size h, and the order q of the local basis functions, when the pollution starts to disappear for the two kinds of local basis functions. The numerical results in the paper will indicate this effect which needs still more rigorous analysis.

The problem of numerical solution is of course related to the implementation. Hence the paper also deals with the quadrature and the *a-posteriori* error estimation. Also here further theoretical analysis is needed.

In this work we study the computational aspects of the q-version of the Partition of Unity Method, which we have also addressed recently in [28] in the context of the *pq*-convergence of the Generalized Finite Element Method, which combines the present approach with the *p*-version of the Finite Element Method. The main differences of the present work with [28] is that here: a) We explore the use of two different local bases, namely the plane-waves also employed in [28], and in addition the wave-bands used by Ladevèze and co-workers [21]–[23] in their approach; b) We also employ semi-analytical tools for all the numerical integrations which allow us to consider cases with many (e.g. six) wavelengths per element. Once more the theoretical basis of our work namely the proofs of existence, uniqueness, and *a-priori* error estimates of q-convergence can be found in Chapter 8 of Melenk [5].

Theory, practical computation and experience are complementary. As was said earlier, the goal of the paper is to stimulate the theoretical questions which would explain various numerical features.

Following this Introduction we summarize the formulation of the Helmholtz equation, its Partition of Unity approximations, we attack the problem of numerical integration of all the integrals employed in the formulation, illustrate the exponential convergence characteristics of the method in the context of two model examples,

and show how it can be explored by extrapolation to obtain easily computable *a-posteriori* error estimates for any computed solution quantity.

2. Theoretical background

In this section we formulate the Helmholtz model problem with Robin boundary conditions in a finite domain and its PUM approximation. We refer the reader to Chapter 8 of [5] for more details and proofs.

Let $\Omega \subset \mathbb{R}^2$ be a bounded domain with boundary $\partial\Omega = \Gamma_1 \cup \Gamma_2$, $\Gamma_1 \cap \Gamma_2 = \emptyset$, as shown in Fig. 1. We will be interested in the solution u of the boundary-value problem

$$(2a) \qquad -\Delta u - k^2 u = f \qquad \text{in } \Omega,$$

$$(2b) \qquad \frac{\partial u}{\partial n} = g_1 \qquad \text{on } \Gamma_1,$$

$$(2c) \qquad \frac{\partial u}{\partial n} - \mathrm{i}ku = g_2 \qquad \text{on } \Gamma_2.$$
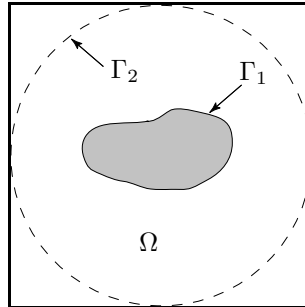
Figure 1. Example of a domain Ω with interior boundary Γ_1 and outer boundary Γ_2.

The weak formulation of (2) is given as follows.
Find $u \in H^1(\Omega)$ such that

$$(3a) \qquad \mathscr{B}(u,v) = \mathscr{L}(v) \quad \forall\, v \in H^1(\Omega)$$

where

$$(3b) \qquad \mathscr{B}(u,v) = \int_\Omega \nabla u \nabla \bar{v}\,\mathrm{d}\Omega - k^2 \int_\Omega u\bar{v}\,\mathrm{d}\Omega + \mathrm{i}k \oint_{\Gamma_2} u\bar{v}\,\mathrm{d}s,$$

$$(3c) \qquad \mathscr{L}(v) = \int_\Omega f\bar{v}\,\mathrm{d}\Omega + \sum_{i=1}^{2} \oint_{\Gamma_i} g_i\bar{v}\,\mathrm{d}s,$$

where $H^1(\Omega)$ is the space of functions with square-integrable derivatives over Ω.

We have from Melenk [5]:

Theorem 1 (Existence and Uniqueness). *Let $f \in H^{-1}(\Omega)$, $g_i \in H^{-1/2}(\Gamma_i)$, $i = 1, 2$. Then there exists a unique solution of the Helmholtz problem which satisfies*

$$(4) \quad \|u\| \overset{\text{def}}{=} \sqrt{\|\nabla u\|_{L^2(\Omega)}^2 + k^2\|u\|_{L^2(\Omega)}^2} \leqslant \mathscr{C}(\Omega, k)\left(\|f\|_{H^{-1}(\Omega)} + \sum_{i=1}^{2} \|g_i\|_{H^{-1/2}(\Gamma_i)} \right).$$

Here $\mathscr{C}(\Omega, k)$ indicates the dependence of $\mathscr{C}$ on the domain Ω and the wave-number k. In the case that Ω is convex, $\mathscr{C}$ does not depend on k.

Let Δ_h be a uniform mesh of squares of size h covering the domain Ω, as is, e.g., shown in Fig. 2(a). Let $\varphi_i^{\Delta_h}$, $i = 1, \ldots$, nnodes, be the classical piecewise bilinear "hat" functions associated with the nodes located at the vertices of the squares (see e.g. Fig. 2 (b)), and let

$$(5) \qquad \omega_i^{\Delta_h} \overset{\text{def}}{=} \operatorname{supp} \varphi_i^{\Delta_h} = \big\{ x \in \Omega \colon \varphi_i^{\Delta_h}(x) > 0 \big\}$$

be the support of $\varphi_i^{\Delta_h}$ which consists of the four squares which share the node as a vertex.
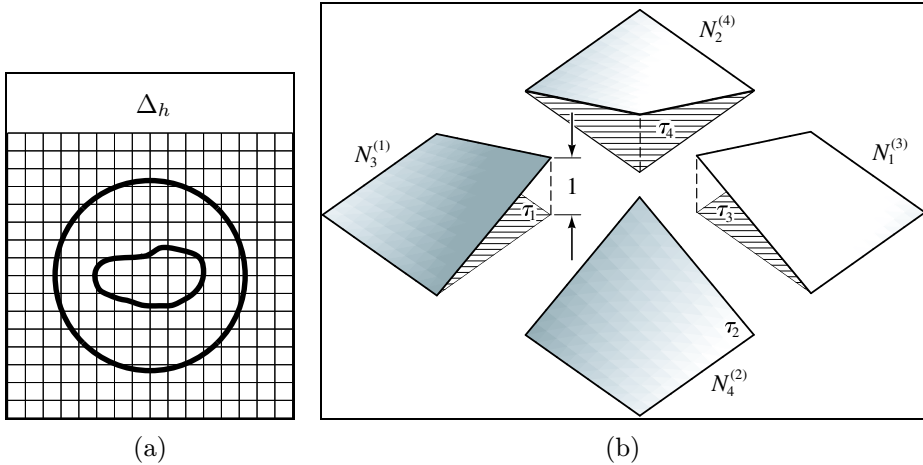
Figure 2. (a) Example of a Cartesian mesh Δ_h used in the formulation of the Partition of Unity Method over the domain Ω. (b) A typical exploded view of a hat function $\varphi_i^{\Delta_h}$ over its support.

We define the Partition of Unity Space:

$$(6) \qquad W_{\Delta_h}^{k;q} = \left\{ v = \sum_{i=1}^{\text{nnodes}} \varphi_i^{\Delta_h} v_i \colon v_i \in W_{\text{loc}}^{k;q}(\omega_i^{\Delta_h}) \right\}$$

where $W_{\text{loc}}^{k;q}$ is the local space of:

a) plane-wave basis functions

$$(7) \quad W_{\text{loc}}^{k;q} = \text{span}\left\{\exp\left(\mathrm{i}k\left(x\cos\frac{2\pi n}{q} + y\sin\frac{2\pi n}{q}\right)\right), \ n = 0,\ldots,q-1\right\},$$

which includes all linear combinations of plane waves travelling in the directions $\left(\cos 2\pi n/q, \sin 2\pi n/q\right)$, $n = 0, \ldots, q-1$.

b) wave-band basis functions

$$(8) \quad W_{\text{loc}}^{k;q} = \text{span}\left\{\int_{\theta_n}^{\theta_{n+1}} \mathrm{e}^{(\mathrm{i}k(x\cos\theta + y\sin\theta))}\,\mathrm{d}\theta\colon\ n = 0,\ldots,q-1, \ \theta_n = \frac{2\pi n - \pi}{q}\right\},$$

which includes all linear combinations of wave-bands obtained by superposition of all the plane waves travelling in the directions $(\cos\theta_n, \sin\theta_n)$ to $(\cos\theta_{n+1}, \sin\theta_{n+1})$, $n = 0, \ldots, q-1$, $\theta_n = (2\pi n - \pi)/q$.

Fig. 3 depicts schematically both the basis functions for $q = 2, 4$ and 6, while Fig. 4 shows the contours of a real part of a discrete plane wave and the corresponding wave-band.
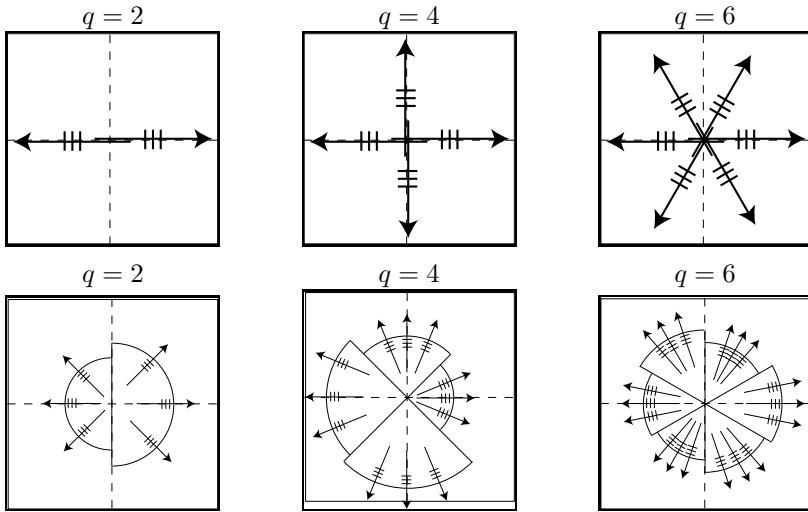

Figure 3. Examples of the employed local basis functions. The top row depicts the plane-wave basis, while the bottom row depicts the wave-band basis for $q = 2, 4$, and 6, respectively.

The PUM solution is defined as follows.

Find

$$(9) \qquad u_h^q = \sum_{i=1}^{\text{nnodes}} \varphi_i^{\Delta h}\left(\sum_{j=1}^{q} a_j^{(i)} W_j^{(i)}\right) \in W_{\Delta_h}^{k;q}$$
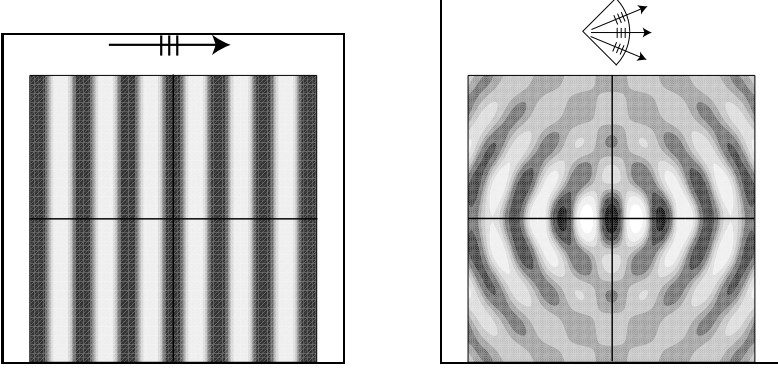
186

Figure 4. Contours of the real part of a) The plane-wave $\exp(\mathrm{i}k(x\cos\theta + y\sin\theta))$ for $\theta = 0$; b) the wave-band $\int_{\theta_1}^{\theta_2} \exp(\mathrm{i}k(x\cos\theta + y\sin\theta))\,\mathrm{d}\theta$ for $\theta_1 = -\pi/4$ and $\theta_2 = \pi/4$.

such that

$$\text{(10)} \qquad \mathscr{B}(u_h^q, v) = \mathscr{L}(v) \quad \forall v \in W_{\Delta_h}^{k;q}$$

where $W_j^{(i)}$, $j = 1, \ldots, q$ are either the plane-wave or wave-band functions employed in the patch $\omega_i^{\Delta h}$.

R e m a r k 1. In [28] we addressed the Generalized Finite Element Method where we seek

$$\text{(11)} \qquad u_h^{p,q} = \sum_{k=1}^{\mathrm{nfem(p)}} b_k N_k + \sum_{i=1}^{\mathrm{nnodes}} \varphi_i^{\Delta h} \left(\sum_{j=1}^q a_j^{(i)} W_j^{(i)} \right) \in S_{h,p}^{k;q} \overset{\text{def}}{=} S_{\Delta_h}^p \oplus W_{\Delta_h}^{k;q}$$

such that

$$\text{(12)} \qquad \mathscr{B}(u_h^{p,q}, v) = \mathscr{L}(v) \quad \forall v \in S_{h,p}^{k;q} \overset{\text{def}}{=} S_{\Delta_h}^p \oplus W_{\Delta_h}^{k;q}$$

where N_k denotes a standard FE bi-p basis functions on Δ_h, nfem(p) is the total number of degrees of freedom for the bi-p FE basis functions, $W_j^{(i)}$, $j = 1, \ldots, q$ are the employed plane wave functions in the patch $\omega_i^{\Delta h}$, and we also discussed the effect of p. In the present paper we let $p = 0$ and consider two possible choices of the local basis functions.

The stability and quasi-optimality of the above PUM approximation of the Helmholtz was proved in [5]. The main result is that

$$\text{(13)} \qquad \|\nabla(u - u_h^q)\|_{L^2(\Omega)} \leqslant \mathscr{C} \inf_{\chi \in S_h^q} \|\nabla(u - \chi)\|_{L^2(\Omega)}$$

where $S_h^q = W_{\Delta h}^{k;q}$, and $\mathscr{C}$ is related to the pollution due to the wave-number.

R e m a r k 2. We will measure the pollution in concrete cases by computing the ratio

$$
(14) \qquad \pi_{S_h^q}(u) = \frac{\|\nabla(u - u_h^q)\|_{L^2(\Omega)}}{\inf\limits_{\chi \in S_h^q} \|\nabla(u - \chi)\|_{L^2(\Omega)}}.
$$

Theorem 2 (q convergence). *Let the solution u of the Helmholtz problem (3) be analytic on $\bar{\Omega} = \Omega \cup \partial\Omega$. Then, for h fixed we have*

$$
(15) \qquad \inf_{\chi \in S_h^q} \|u - \chi\| \leqslant \mathscr{C}(h) e^{-\alpha q}
$$

where α depends on h.

The main results needed for the proof of (15) are given in Sections 8.4–8.6 of Melenk [5].

3. Numerical integration

In [28] we used Gauss-Legendre numerical integration to evaluate all integrals. Here, in the case of plane-waves, we will employ a semi-analytical scheme which follows from [13], [14].

Noting that a plane wave function $W_j^{(m)}(\mathbf{x}) = \exp(ik\mathbf{x} \cdot \mathbf{e}_j)$ satisfies

$$
(16) \qquad \nabla W_m^{(j)} = ik\mathbf{e}_m W_m^{(j)}
$$

we write the typical element of the stiffness matrix

$$
(17) \qquad \int_\tau \nabla(\varphi_r^{\Delta h} W_m^{(r)}) \cdot \nabla(\varphi_s^{\Delta h} W_n^{(s)}) - k^2(\varphi_r^{\Delta h} W_m^{(r)})(\varphi_s^{\Delta h} W_s^{(s)}) \, \mathrm{d}\tau
$$

into the form

$$
(18) \qquad \int_\tau \exp(ik(\mathbf{e}_m + \mathbf{e}_n) \cdot \mathbf{x})[(\nabla\varphi_r^{\Delta h} + ik\mathbf{e}_m \varphi_r^{\Delta h}) \cdot (\nabla\varphi_s^{\Delta h} + ik\mathbf{e}_n \varphi_s^{\Delta h}) - k^2 \varphi_r^{\Delta h} \varphi_s^{\Delta h} \, \mathrm{d}\tau].
$$

Next we employ the Filon integration rule (see [29, p. 151]) to evaluate (18). Recall that Filon's rule is used to integrate highly-oscillatory integrals in the form

$$
(19) \qquad \int_a^b f(t) \cos kt \, \mathrm{d}t \quad \text{and} \quad \int_a^b f(t) \sin kt \, \mathrm{d}t
$$

by subdividing the interval $[a, b]$ into $2N$ subintervals of equal length and approximating $f(t)$ by a parabola obtained by interpolating $f(t)$ at mesh points. For rectangular

element τ, the integral (18) can be written as an iterated integral in the x and y directions. Further, $\varphi_r^{\Delta h}(x, y) = \varphi_r^{\Delta h}(x)\varphi_r^{\Delta h}(y)$ and thus (18) can be split into two 1-D integrals. For example, we have

$$(20) \qquad \frac{\partial}{\partial x}\varphi_r^{\Delta h}(x, y)\frac{\partial}{\partial x}\varphi_s^{\Delta h}(x, y) = \frac{\partial}{\partial x}\varphi_r^{\Delta h}(x)\frac{\partial}{\partial x}\varphi_s^{\Delta h}(x)\varphi_r^{\Delta h}(y)\varphi_s^{\Delta h}(y),$$
$$= F(x)G(y)$$

which, after multiplication by $\exp(\mathrm{i}k(\mathbf{e}_m + \mathbf{e}_n) \cdot \mathbf{x})$ can be written as

$$(21) \qquad \int_I \cos(\omega_1 x)F(x)\,\mathrm{d}x \int_J \cos(\omega_2 y)G(y)\,\mathrm{d}y$$
$$- \int_I \sin(\omega_1 x)F(x)\,\mathrm{d}x \int_J \sin(\omega_2 y)G(y)\,\mathrm{d}y$$
$$+ \mathrm{i} \int_I \sin(\omega_1 x)F(x)\,\mathrm{d}x \int_J \cos(\omega_2 y)G(y)\,\mathrm{d}y$$
$$+ \mathrm{i} \int_I \cos(\omega_1 x)F(x)\,\mathrm{d}x \int_J \sin(\omega_2 y)G(y)\,\mathrm{d}y$$

with $\omega_1 = k(\cos\theta_m + \cos\theta_n)$ and $\omega_2 = k(\sin\theta_m + \sin\theta_n)$, and each one of the 1-D integrals can be evaluated by Filon's rule.

We performed some computational experiments with $\tau = (0, 1) \times (0, 1)$ and $k = 20$, and computed the stiffness matrix using 40×40 Gauss Legendre Quadrature and Filon's rule with 2 subintervals on x and y coordinates. Analyzing the results for $q = 2, 4, 6, \ldots, 40$ we found that for $k = 20$ both the quadratures give indentical results up to the roundoff error, while Filon's rule is always more economical as shown in Fig. 5.

In the case of wave-bands, we use $(40 \times 40)^2$ Gauss integration rule; more precisely we use the 40×40 Gauss rule over τ and the 40 point Gauss rule in each band. For example,

$$(22) \qquad \int_\tau k^2 \left(\varphi_r^{\Delta h} \int_{\theta_{r_1}}^{\theta_{r_2}} \mathrm{e}^{\mathrm{i}k(x\cos\theta + y\sin\theta)}\,\mathrm{d}\theta \right) \left(\varphi_s^{\Delta h} \int_{\theta_{s_1}}^{\theta_{s_2}} \mathrm{e}^{\mathrm{i}k(x\cos\theta + y\sin\theta)}\,\mathrm{d}\theta \right) \mathrm{d}\tau$$

is computed by

$$(23) \qquad \sum_{i=1}^{40}\sum_{j=1}^{40} k^2 \hat{\varphi}_r^{\Delta h}(\xi_i, \xi_j)\hat{\varphi}_s^{\Delta h}(\xi_i, \xi_j)|J|w_i w_j$$
$$\sum_{m=1}^{40} \exp\big(\mathrm{i}k(x(\xi_i)\cos\theta(\xi_m) + y(\xi_j)\sin\theta(\xi_m))\big) \cdot \tfrac{1}{2}(\theta_{r_2} - \theta_{r_1})w_m$$
$$\sum_{n=1}^{40} \exp\big(\mathrm{i}k(x(\xi_i)\cos\theta(\xi_n) + y(\xi_j)\sin\theta(\xi_n))\big) \cdot \tfrac{1}{2}(\theta_{s_2} - \theta_{s_1})w_n$$
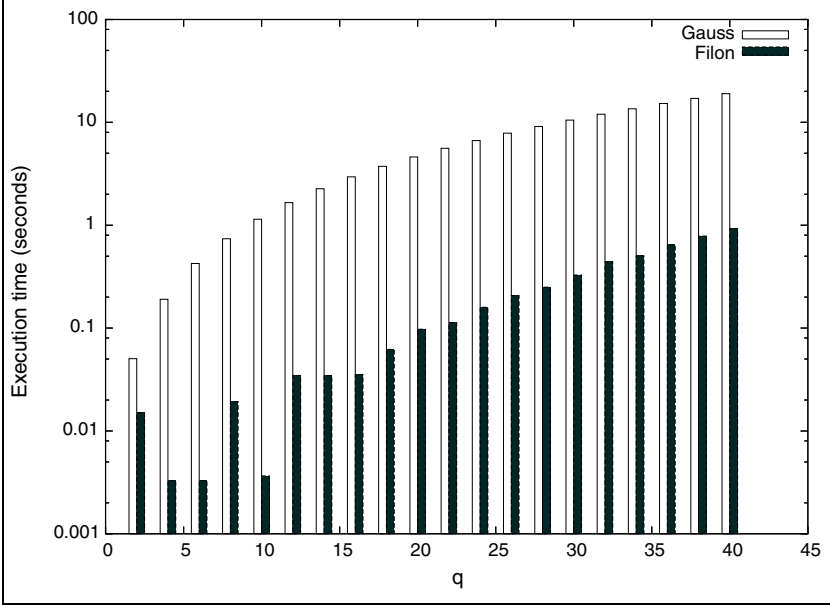
Figure 5. Comparison of execution time for computation of stiffness matrices between Gauss Legendre integration and Filon integration.

where ξ_i and w_i are the Gauss Legendre points and the weights, respectively, and $\hat{\varphi}_s^{\Delta h}$ is the piecewise bilinear "hat" function in the master domain $(1,1) \times (-1,1)$. A more economical semi-analytical approach for evaluating the integrals in the case of wave-bands has been proposed by Ladevèze and Rouch [23].

4. Discussion of the computed results

4.1. Plane Wave on Rectangular Domain

As our first example, we took the Helmholtz equation on the unit square $\Omega = (0,1) \times (0,1)$ with Robin boundary conditions:

$$\Delta u + k^2 u = 0 \quad \text{in } \Omega, \tag{24a}$$

$$\frac{\partial u}{\partial n} + \mathrm{i}ku = g \quad \text{on } \partial\Omega \tag{24b}$$

where we chose g such that the exact solution is the plane wave

$$u(x,y) = \mathrm{e}^{\mathrm{i}k(x\cos\theta + y\sin\theta)}, \quad \theta = \frac{\pi}{16}. \tag{25}$$

Here we let $k = 20$ and employ uniform $N \times N$ meshes of squares for $N = 1, 2, 4,$ and 8 denoted respectively as mesh A, mesh B, mesh C, and mesh D. Tab. 1

summarizes the data for the meshes employed: their mesh size h and the respective Number of Waves Per Element (NWPE): $h/\lambda = hk/2\pi$.

	N	h	NWPE
Mesh A	1	1.0	3.18
Mesh B	2	0.5	1.59
Mesh C	4	0.25	0.80
Mesh D	8	0.125	0.40

Table 1. Meshes utilized in the analysis: N is the number of elements in the x and y directions, h is the uniform mesh size, and NWPE is the Number of Waves Per Element.

Fig. 6 plots the percent relative error in the H^1-seminorm with respect to the square root of the total number of degrees of freedom $\sqrt{\text{NDOF}}$ in the horizontal axis. Here we can see that asymptotically we obtain in both cases exponential convergence:

$$(26) \qquad \|\nabla(u - u_h^q)\| \approx \mathscr{C} e^{-\gamma \sqrt{\text{NDOF}}}$$

where $\mathscr{C}$ depends on h. It is noteworthy that in the pre-asymptotic range the PUM with plane-waves delivers much better accuracy than the PUM with wave-bands, especially as the mesh is refined.
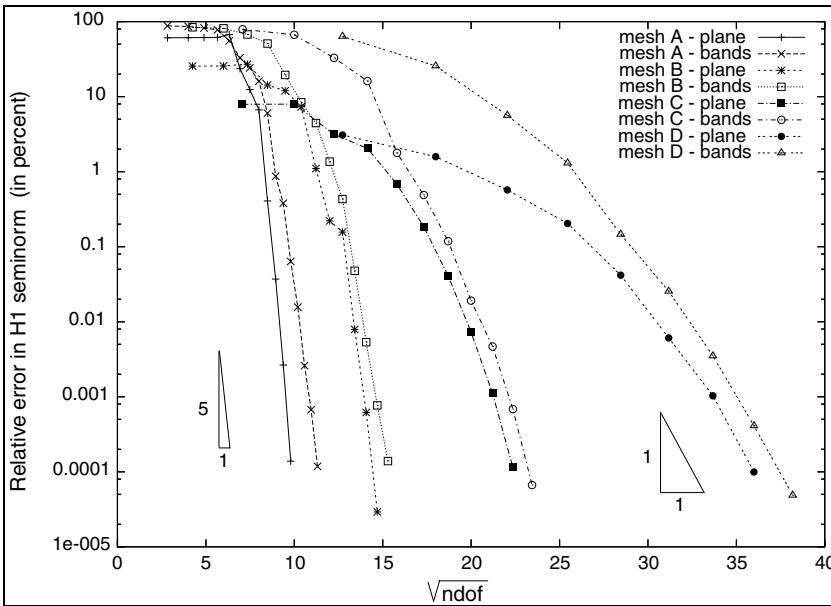

Figure 6. q-convergence of the PUM using plane-wave and wave-band functions for Mesh A, B, C, and D.

q	Mesh A		Mesh B		Mesh C		Mesh D	
	plane	bands	plane	bands	plane	bands	plane	bands
2	.4804E+2 (1.2656)	.8673E+2 (1.0123)	.1991E+2 (1.2848)	.8047E+2 (1.0461)	.6740E+1 (1.1723)	.6768E+2 (1.1674)	.2899E+1 (1.0617)	.3725E+2 (1.7044)
4	.4804E+2 (1.2733)	.8312E+2 (1.0367)	.1982E+2 (1.2911)	.7108E+2 (1.1456)	.6499E+1 (1.2267)	.4382E+2 (1.5224)	.1530E+1 (1.0333)	.1980E+2 (1.2924)
6	.4784E+2 (1.2837)	.7096E+2 (1.1598)	.1805E+2 (1.5014)	.4562E+2 (1.4796)	.2898E+1 (1.0849)	.2084E+2 (1.5763)	.5649E+0 (1.0110)	.5031E+1 (1.1175)
8	.4625E+2 (1.3328)	.5731E+2 (1.3551)	.7638E+1 (1.8657)	.3248E+2 (1.5727)	.1963E+1 (1.0413)	.7755E+1 (2.0812)	.2036E+0 (1.0025)	.1276E+1 (1.0219)
10	.3085E+2 (2.1812)	.3296E+2 (1.6811)	.4529E+1 (2.6496)	.9547E+1 (2.0383)	.6265E+0 (1.0817)	.1680E+1 (1.0589)	.4171E-1 (1.0012)	.1460E+0 (1.0034)
12	.1435E+2 (1.6432)	.2343E+2 (1.4063)	.2794E+1 (2.6249)	.3684E+1 (2.2801)	.1832E+0 (1.0153)	.4780E+0 (1.0201)	.6085E-2 (1.0015)	.2551E-1 (1.0027)
14	.5856E+1 (2.1209)	.1316E+2 (1.8404)	.7339E+0 (1.5043)	.1618E+1 (2.7466)	.4013E-1 (1.0125)	.1173E+0 (1.0119)	.1033E-2 (1.0010)	.3496E-2 (1.0014)
16	.1770E+1 (3.7616)	.5150E+1 (3.1204)	.1674E+0 (1.3202)	.8736E+0 (1.5545)	.7176E-2 (1.0111)	.1890E-1 (1.0064)	.9904E-4 (1.0026)	.4094E-3 (1.0007)
18	.3616E+0 (1.1258)	.1392E+1 (4.3197)	.3489E-1 (4.4855)	.1903E+0 (2.2648)	.1099E-2 (1.0055)	.4635E-2 (1.0080)		.4858E-4 (1.0016)
20	.3653E-1 (1.0151)	.3663E+0 (2.3713)	.7387E-2 (1.0700)	.3766E-1 (1.2690)	.1132E-3 (1.0133)	.6812E-3 (1.0060)		
22	.2615E-2 (1.0134)	.1123E+0 (3.3856)	.5557E-3 (1.1110)	.5128E-2 (1.0429)		.6593E-4 (1.0102)		
24	.1375E-3 (1.0058)	.3232E-1 (1.9706)	.2834E-4 (1.0296)	.7461E-3 (1.0288)				
26		.1024E-1 (1.5303)		.1354E-3 (1.0258)				
28		.2311E-2 (1.1255)						
30		.6362E-3 (1.0544)						
32		.1157E-3 (1.0225)						

Table 2. The values of the percent relative error in the best approximation $\|\nabla(u - \mathscr{A}_h^q u)\|_{L^2(\Omega)}/\|\nabla u\|_{L^2(\Omega)} \times 100\,\%$ using the plane-wave and wave-band functions. The number inside the bracket is the pollution ratio $\pi_{S_h^q}(u)$, namely the ratio between the percent relative error of the PUM and the best approximation.

q	Mesh A		Mesh B		Mesh C		Mesh D	
	plane	bands	plane	bands	plane	bands	plane	bands
2	$.7258E{+}2$	$.3489E{+}2$	$.4037E{+}2$	$.1520E{+}2$	$.2386E{+}2$	$.1101E{+}2$	$.1146E{+}2$	$.8322E{+}1$
	(1.1730)	(1.0957)	(1.2527)	(1.0579)	(1.2871)	(1.0836)	(1.1536)	(1.4215)
4	$.7246E{+}2$	$.2851E{+}2$	$.3968E{+}2$	$.1198E{+}2$	$.2123E{+}2$	$.5751E{+}1$	$.4728E{+}1$	$.3786E{+}1$
	(1.1736)	(1.2936)	(1.2679)	(1.4349)	(1.4932)	(1.7736)	(1.0992)	(1.6302)
6	$.7114E{+}2$	$.1110E{+}2$	$.2613E{+}2$	$.5189E{+}1$	$.5917E{+}1$	$.2284E{+}1$	$.1185E{+}1$	$.6250E{+}0$
	(1.2003)	(1.3802)	(1.9644)	(2.6768)	(1.1256)	(1.5639)	(1.0118)	(1.1162)
8	$.6081E{+}2$	$.8525E{+}1$	$.7795E{+}1$	$.5413E{+}1$	$.1913E{+}1$	$.1836E{+}1$	$.2475E{+}0$	$.2463E{+}0$
	(1.2263)	(1.9132)	(1.3765)	(1.9656)	(1.0538)	(14.336)	(1.0016)	(1.0154)
10	$.3556E{+}2$	$.8341E{+}1$	$.4654E{+}1$	$.4028E{+}1$	$.5796E{+}0$	$.6442E{+}0$	$.3747E{-}1$	$.5907E{-}1$
	(2.3332)	(1.7995)	(1.0765)	(1.8841)	(1.0851)	(1.1956)	(1.0011)	(1.0242)
12	$.1477E{+}2$	$.6529E{+}1$	$.2303E{+}1$	$.1845E{+}1$	$.1561E{+}0$	$.1067E{+}0$	$.5026E{-}2$	$.7836E{-}2$
	(1.7258)	(1.5944)	(2.1806)	(8.0000)	(1.0167)	(1.0309)	(1.0012)	(1.0046)
14	$.3811E{+}1$	$.3451E{+}1$	$.5460E{+}0$	$.3458E{+}0$	$.2860E{-}1$	$.2460E{-}1$	$.7434E{-}3$	$.7177E{-}3$
	(1.9234)	(2.8708)	(2.0751)	(1.5058)	(1.0157)	(1.0171)	(1.0019)	(1.0022)
16	$.1175E{+}1$	$.1771E{+}1$	$.1805E{+}0$	$.1500E{+}0$	$.5533E{-}2$	$.7578E{-}2$	$.7716E{-}4$	$.1250E{-}3$
	(3.9566)	(2.4032)	(1.0820)	(1.4767)	(1.0074)	(1.0227)	(0.9999)	(1.0008)
18	$.5348E{+}0$	$.6593E{+}0$	$.5723E{-}1$	$.4223E{-}1$	$.1418E{-}2$	$.1072E{-}2$		
	(1.1887)	(4.6519)	(10.666)	(1.0992)	(1.0085)	(1.0075)		
20	$.8084E{-}1$	$.1250E{+}0$	$.1443E{-}1$	$.9467E{-}2$	$.2430E{-}3$	$.1942E{-}3$		
	(1.0143)	(3.4384)	(1.0804)	(1.1049)	(1.0325)	(1.0051)		
22	$.2748E{-}1$	$.2894E{-}1$	$.4479E{-}2$	$.2362E{-}2$				
	(1.0124)	(1.5463)	(1.0554)	(1.0868)				
24	$.7721E{-}2$	$.2005E{-}1$	$.1527E{-}2$	$.9474E{-}3$				
	(1.0060)	(1.1546)	(1.0308)	(1.0278)				
26	$.2357E{-}2$	$.9657E{-}2$	$.5843E{-}3$	$.3069E{-}3$				
	(1.0076)	(1.3410)	(1.0199)	(1.0713)				
28	$.7026E{-}3$	$.4007E{-}2$	$.2269E{-}3$					
	(1.0080)	(1.0177)	(1.0220)					
30	$.3876E{-}3$	$.1582E{-}2$						
	(0.5575)	(1.0076)						

Table 3. The values of the percent relative error in the best approximation $\|\nabla(u - \mathscr{A}_h^q u)\|_{L^2(\Omega)} / \|\nabla u\|_{L^2(\Omega)} \times 100\%$ using the plane-wave and wave-band functions for the domain Ω_1. The number inside the bracket is the pollution ratio $\pi_{S_h^q}(u)$, namely the ratio between the percent relative error of the PUM and the best approximation.

Tab. 2 gives the values of the percent relative error in the best approximation: $\|\nabla(u - \mathscr{A}_h^q u)\|_{L^2(\Omega)} / \|\nabla u\|_{L^2(\Omega)} \times 100\,\%$, where $\mathscr{A}_h^q u \in S_h^q$ is such that

$$(27) \qquad \int_\Omega \nabla(\mathscr{A}_h^q u) \cdot \nabla \overline{v} \, \mathrm{d}\Omega = \int_\Omega \nabla u \cdot \nabla \overline{v} \, \mathrm{d}\Omega \quad \forall v \in S_h^q$$

where u is the analytical solution given by (25). Tab. 2 also gives the value of the pollution ratio $\pi_{S_h^q}(u)$ in each case. The deviation of $\pi_{S_h^q}(u)$ from the value one is the measure of the pollution.

Fig. 7 and Fig. 8 show the graph of the percent relative error in the PUM solution and the best approximation for the plane-wave and the wave-bands PUM space, respectively. We can see from both figures that for sufficiently high q depending on h, the solution converges exponentially as

$$(28) \qquad \|\nabla(u - u_h^q)\| \approx \mathscr{C}_1 \mathrm{e}^{-\beta q}$$

with the same rate $\beta \approx 1$. Note also that as the mesh is refined, the effect of the pollution is practically negligible almost starting from $q = 2$.

In summary, it seems that for the problem with the exact solution given by (25) the PUM using plane-waves performs better than the PUM using wave-bands especially for small h and high q. For large h and low q the PUM using bands has smaller pollution ratio. The better performace of the PUM using plane-waves can be partially explained from the fact that the exact solution is also a plane wave.

4.2. Rigid scattering problem

We obtained our second example by employing the analytical solution of scattering of a plane wave by a rigid circular cylinder, which is depicted in Fig. 9. Employing cylindrical coordinates (r, θ), the boundary value problem for the scattered pressure $u(r, \theta)$ reads

$$(29a) \qquad \Delta u + k^2 u = 0, \quad r > a,$$

$$(29b) \qquad \frac{\partial u}{\partial r} = -\frac{\partial}{\partial r}(u_{\mathrm{inc}}), \quad r = a,$$

$$(29c) \qquad \lim_{r \to \infty} \sqrt{r}\Big(\frac{\partial u}{\partial r} - \mathrm{i}ku\Big) = 0$$

where

$$(30) \qquad u_{\mathrm{inc}}(r, \theta) = P_0 \mathrm{e}^{\mathrm{i}kr \cos \theta}$$
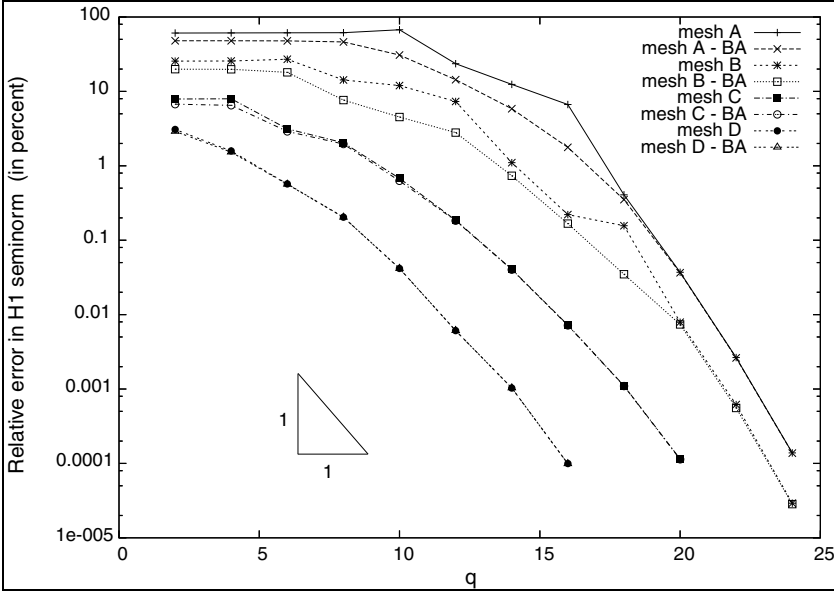
194

Figure 7. q-convergence of the PUM and the best approximation for Mesh A, B, C, and D computed using plane-wave functions.
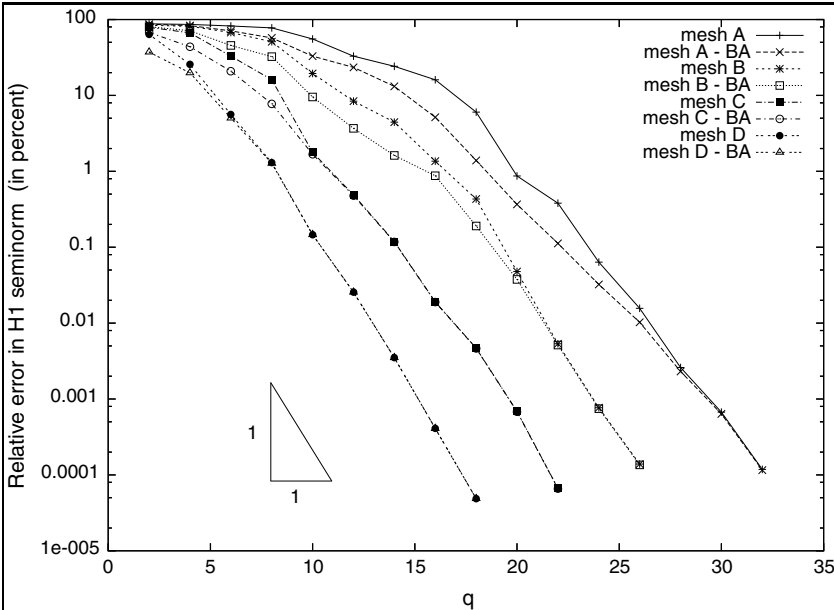

Figure 8. q-convergence of the PUM and best approximation for Mesh A, B, C, and D computed using wave-bands functions.
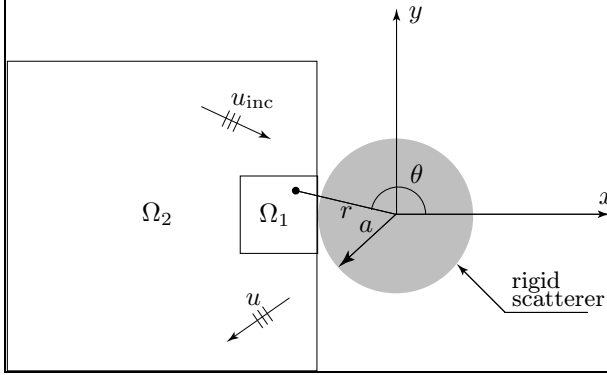
Figure 9. Notations used in the definition of the model example of scattering of a plane wave by a rigid circular scatterer and the problem domains Ω_i.

is the pressure field for the incident plane wave. Using separation of variables (see, e.g., [30, p. 412]) we obtain

$$(31) \qquad u(r,\theta) = -P_0 \sum_{n=0}^{\infty} \varepsilon_n \mathrm{i}^n \frac{J_n'(ka)H_n(kr)}{H_n'(ka)} \cos(n\theta)$$

where $\varepsilon_0 = 1$, $\varepsilon_n = 2$, $n \neq 0$, $H_n(z)$ is the cylindrical Hankel function of the first kind, and $J_n(z)$ is the cylindrical Bessel function of the first kind. We set our example problem in square domains Ω_i, $i = 1, 2$, adjacent to the scatterer and employed (31) to obtain g on $\partial\Omega_i$.
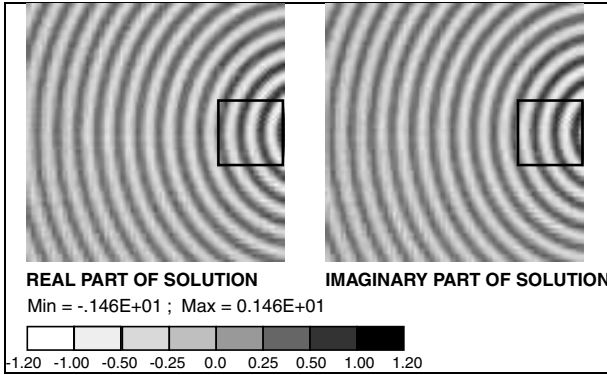

Figure 10. Contours of the real and imaginary part of the scattered field in Ω_2. The small box inside the contours is the domain Ω_1.

In our computations we employed $k = 20$ and domains $\Omega_1 = (-2, -1) \times (-0.5, 0.5)$ and $\Omega_2 = (-5, -1) \times (-2, 2)$. As in the previous example, we employed uniform meshes of squares obtained from nested refinements of the domains Ω_i.

196

Fig. 11 reports the convergence of the H^1-seminorm of the error with increasing q using the domain Ω_1. Note that for this example the PUM with wave-bands gives better accuracy in the pre-asymptotic range as compared with the PUM with plane-waves. Asymptotically, both choices give almost identical accuracies converging exponentially with respect to $\sqrt{\text{NDOF}}$.
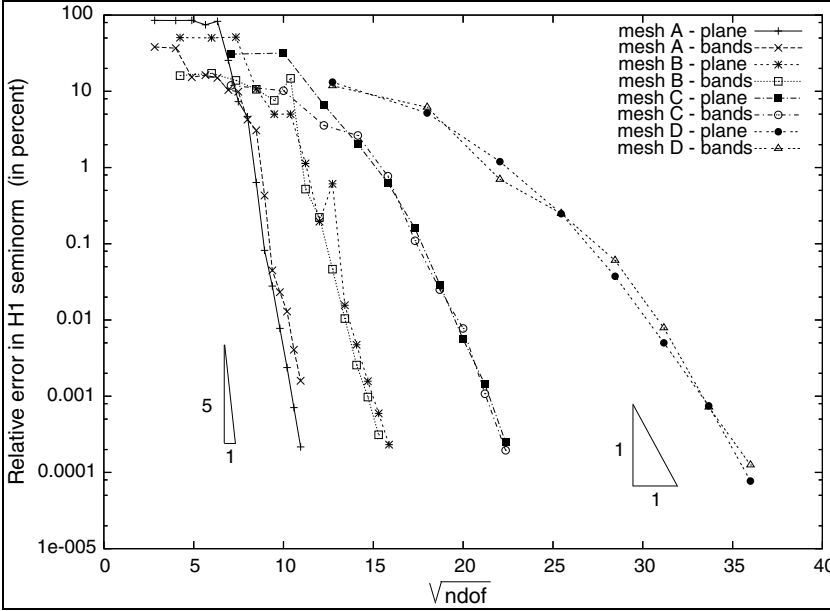

Figure 11. q-convergence of the PUM using plane-wave and wave-band functions for domain Ω_1 using Mesh A, B, C, and D.

Fig. 12 and Fig. 13 plot the percent relative error in the PUM solution versus the corresponding error in the best approximation for the plane-wave and wave-band bases, respectively, using the domain Ω_1. Once more we see that we get exponential convergence with respect to q, for sufficently high q depending on h with rate $\beta \approx 1$.

In Fig. 14 we plot the result of computation on the domain Ω_2 using a uniform 2×2 mesh, such that the Number of Waves Per Element NPWE ≈ 6.37, while in Fig. 15 we also include the results for the 4×4 mesh for which NPWE ≈ 3.18. Note that the pollution is significant for both bases and for almost the entire range of q for both meshes, and that the rate of exponential convergence improves as the mesh is refined.

From the above results we see that for "smooth" solutions, the PUM with wave-bands performs better than with plane-waves while stability is the same for both bases. Theoretical understanding is not available although the smoothness of the
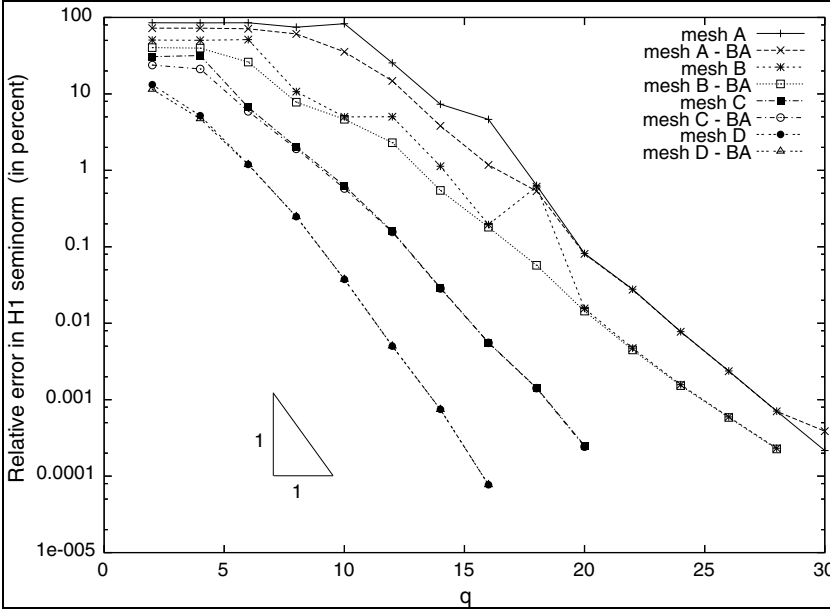
Figure 12. q-convergence of the PUM and the best approximation for the domain Ω_1 using Mesh A, B, C, and D computed using plane-wave functions.
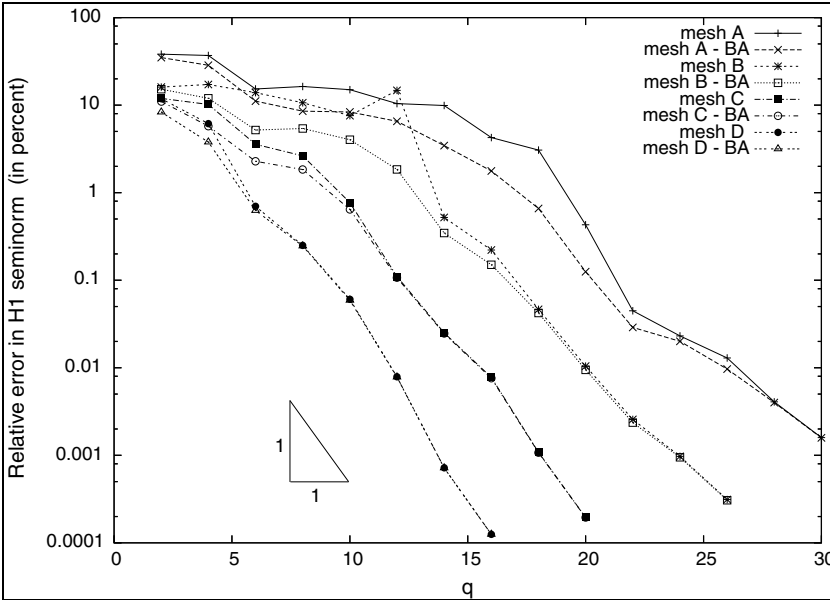

Figure 13. q-convergence of the PUM and the best approximation for the domain Ω_1 using Mesh A, B, C, and D computed using wave-bands functions.
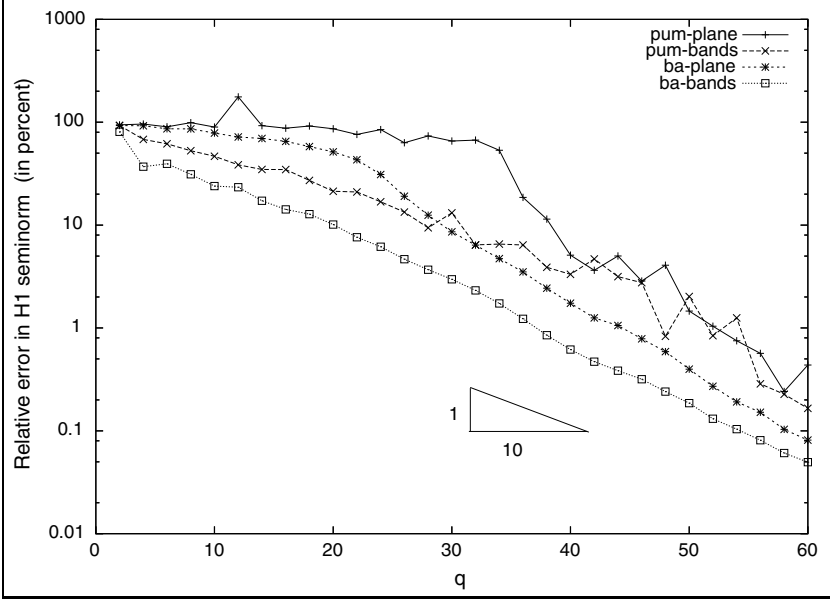
198

Figure 14. q-convergence of the PUM and the best approximation for the domain Ω_2 using uniform 2×2 mesh computed using plane-wave and wave-bands functions.

solution obviously plays a role. The problem relates to the approximation properties of the basis functions employed on the circle of the Fourier symbol of the equation.

4.3. A-posteriori error estimation by q-extrapolation

The exponential rate of convergence of the PUM solution with respect to q enables us to use a simple a-posteriori error estimation by extrapolation as outlined in [31]. Another approach for *a-posteriori* estimation of PUM can be found in [32].

Assuming that the quantity of interest converges exponentially exactly like (28) we have

$$(32) \qquad \log \frac{\mathscr{F}(u) - \mathscr{F}(u_h^q)}{\mathscr{F}(u) - \mathscr{F}(u_h^{q-2})} \approx \log \frac{\mathrm{e}^{-\beta q}}{\mathrm{e}^{-\beta(q-2)}} = -2\beta,$$

which gives us the ability to estimate the exact quantity of interest $\mathscr{F}(u)$ by solving the linear equation

$$(33) \qquad \frac{\tilde{\tilde{\mathscr{F}}}(u) - \mathscr{F}(u_h^q)}{\tilde{\tilde{\mathscr{F}}}(u) - \mathscr{F}(u_h^{q-2})} = \frac{\tilde{\tilde{\mathscr{F}}}(u) - \mathscr{F}(u_h^{q-2})}{\tilde{\tilde{\mathscr{F}}}(u) - \mathscr{F}(u_h^{q-4})}$$

199
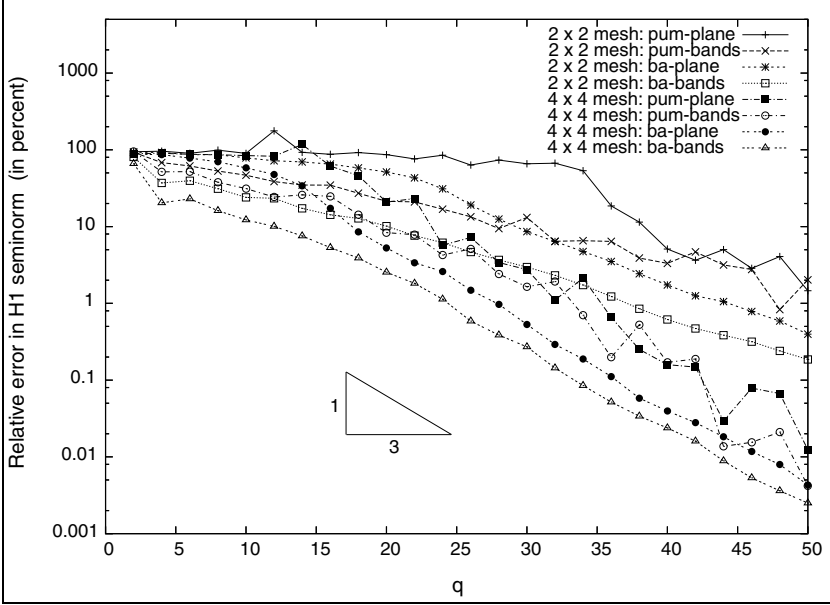
Figure 15. *q*-convergence of the PUM and the best approximation for the domain Ω_2 using uniform 2×2 and 4×4 mesh computed using plane-wave and wave-bands functions.

and hence

$$(34) \qquad \tilde{\mathscr{F}}(u) = \frac{-\mathscr{F}^2(u_h^{q-2}) + \mathscr{F}(u_h^q)\mathscr{F}(u_h^{q-4})}{\mathscr{F}(u_h^q) + \mathscr{F}(u_h^{q-4}) - 2\mathscr{F}(u_h^{q-2})}$$

where $\tilde{\mathscr{F}}(u)$ is the *q*-extrapolated estimate for $\mathscr{F}(u)$.

As an example, consider the rigid scattering problem and let us employ the modulus of the solution on the surface of the scatterer coinciding with the domain boundary as the quantity of interest, namely $\mathscr{F}(u) = |u(-a, 0)|$.

Mesh	plane-wave basis	wave-band basis
A	1.088107	1.088061
B	1.088040	1.088040
C	1.088040	1.088044
D	1.088040	1.088039

Table 4. The extrapolated estimate $\tilde{\mathscr{F}}(u)$ for Mesh A, B, C, and D using both the plane-wave and the wave-band basis function.

Fig. 16 and Fig. 17 shows the graphs of the output $\mathscr{F}(u_h^q)$ respectively for the plane-wave and the wave-bands PUM basis versus *q*. From both figures we can see that the finer mesh reaches the asymptotic range faster than the coarser one.
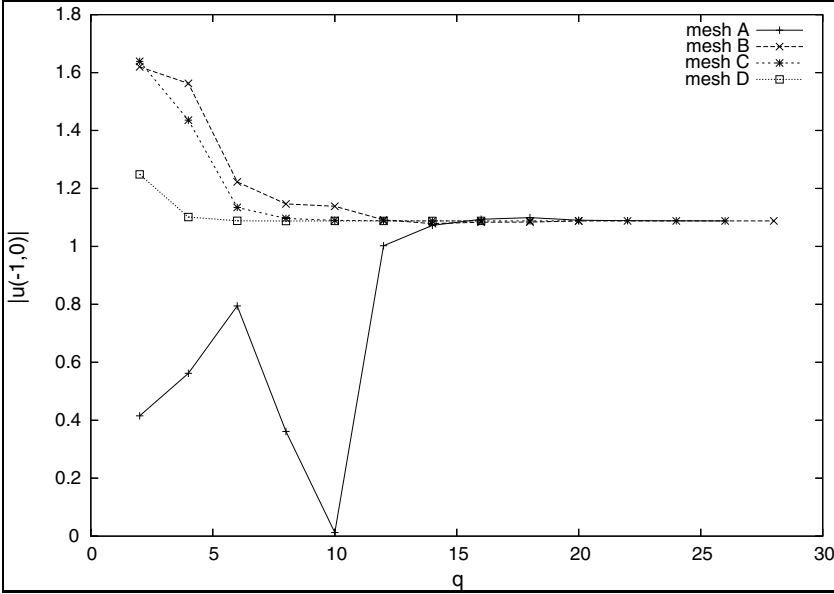
200

Figure 16. Graph of the output $\mathscr{F}(u_h^q) = |u_h^q(-a, 0)|$ on Mesh A, B, C, and D using plane-wave basis functions.
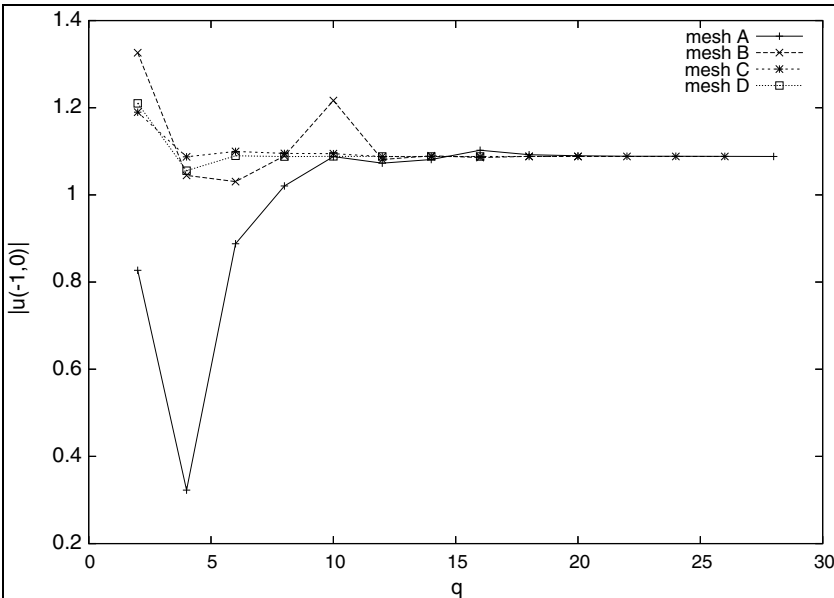

Figure 17. Graph of the output $\mathscr{F}(u_h^q) = |u_h^q(-a, 0)|$ on Mesh A, B, C, and D using wave-band basis functions.

Using the same values of q as in Figs. 16 and 17, we report the exact and estimated quantity of interest for $\mathscr{F}(u_h^{q-4})$ in Tab. 5. We can see that we get very good effectivity indices for all the meshes and for both types of basis functions.

Mesh	special function	$\dfrac{|\mathscr{F}(u) - \mathscr{F}(u_h^{q-4})|}{\mathscr{F}(u)}$	$\dfrac{|\tilde{\mathscr{F}}(u) - \mathscr{F}(u_h^{q-4})|}{\tilde{\mathscr{F}}(u)}$	θ
A	plane-waves	0.0669 %	0.0607 %	0.9073
	wave-bands	0.0493 %	0.0473 %	0.9594
B	plane-waves	0.0014 %	0.0014 %	1.0000
	wave-bands	0.0031 %	0.0083 %	2.6774
C	plane-waves	0.0051 %	0.0051 %	1.0000
	wave-bands	0.0004 %	0.0007 %	1.7500
D	plane-waves	0.0009 %	0.0009 %	1.0000
	wave-bands	0.0027 %	0.0026 %	0.9630

Table 5. Exact and estimated value of the quantity of interest and its effectivity index for Mesh A, B, C, and D computed using PUM with the plane-waves and wave-bands.

5. Conclusions

The goal of the paper was to study numerically the PUM for the Helmholtz equation, the effect of the choice of the local basis functions, the quadrature, and the *a-posteriori* error estimation. Two kinds of local basis functions were considered, namely the plane-waves and the wave-bands. The conclusions are:

1. There is no big difference in the performance of the PUM with either kind of local basis. Nevertheless, various theoretical questions still exist. From the practical point of view the plane-waves are preferable because of the low cost of the numerical quadrature.
2. There is need for theoretical analysis of the (disappearance of) pollution with h and q.
3. The *a-posteriori* error estimation based on q-extrapolation has similar effectiveness as in the elasticity computations where it is used in the context of commercial *p*-version finite element codes. The *a-posteriori* error estimates can also be used to find out when the pollution becomes negligible in the particular case.
4. For the PUM using plane-waves on rectangular elements, a semi-analytical approach based on the Filon rule is rather effective. Further work is needed for the case of wave-bands.

References

[1] *I. Babuška, G. Caloz, and J. E. Osborn*: Special finite element methods for a class of second order elliptic problems with rough coefficients. SIAM J. Numer. Anal. *31* (1994), 945–981.   Zbl 0807.65114

[2] *J. M. Melenk, I. Babuška*: Approximation with harmonic and generalized harmonic polynomials in the partition of unity method. Comput. Assist. Mech. Eng. Sci. *4* (1997), 607–632.   Zbl 0951.65128

[3] *J. M. Melenk, I. Babuška*: The partition of unity finite element method: Basic theory and applications. Comput. Methods Appl. Mech. Eng. *139* (1996), 289–314.
                                                                                                Zbl 0881.65099

[4] *I. Babuška, J. M. Melenk*: The partition of unity method. Int. J. Numer. Methods. Eng. *40* (1997), 727–758.   Zbl 0949.65117

[5] *J. M. Melenk*: On generalized finite element methods. PhD. thesis. University of Maryland, 1995.

[6] *I. Babuška, T. Strouboulis, and K. Copps*: The design and analysis of the generalized finite element method. Comput. Methods Appl. Mech. Eng. *181* (2000), 43–69.
                                                                                                Zbl 0983.65127

[7] *T. Strouboulis, I. Babuška, and K. Copps*: The generalized finite element method: An example of its implementation and illustration of its performance. Int. J. Numer. Methods Eng. *47* (2000), 1401–1417.   Zbl 0955.65080

[8] *T. Strouboulis, K. Copps, and I. Babuška*: The generalized finite element method. Comput. Methods Appl. Mech. Eng. *190* (2001), 4081–4193.   Zbl 1997.74069

[9] *T. Strouboulis, L. Zhang, and I. Babuška*: Generalized finite element method using mesh-based handbooks: Application to problem in domains with many voids. Comput. Methods Appl. Mech. Eng. *192* (2003), 3109–3161.   Zbl 1054.74059

[10] *T. Strouboulis, L. Zhang, and I. Babuška*: p-version of the generalized FEM using mesh-based handbooks with applications to multiscale problems. Int. J. Numer. Methods Eng. *60* (2004), 1639–1672.   Zbl 1059.65106

[11] *N. Sukumar, D. L. Chopp, N. Moës, and T. Belytschko*: Modeling holes and inclusions by level sets in the extended finite element method. Comput. Methods Appl. Mech. Eng. *190* (2001), 6183–6200.   Zbl 1029.74049

[12] *O. Laghrouche, P. Bettess*: Solving short wave problems using special finite elements—towards an adaptive approach. In: The Mathematics of Finite Elements and Applications X (J. R. Whiteman, ed.). Elsevier, Amsterdam, 1999, pp. 181–194.
                                                                                                Zbl 0960.65122

[13] *P. Bettess, J. Shirron, O. Laghrouche, B. Peseux, R. Sugimoto, and J. Trevelyan*: A numerical integration scheme for special finite elements for the Helmholtz equation. Int. J. Numer. Methods Eng. *56* (2003), 531–552.   Zbl 1022.65126

[14] *R. Sugimoto, P. Bettess, and J. Trevelyan*: A numerical integration scheme for special quadrilateral finite elements for the Helmholtz equation. Commun. Numer. Methods Eng. *19* (2003), 233–245.   Zbl 1016.65087

[15] *E. Perrey-Debain, O. Laghrouche, P. Bettess, and J. Trevelyan*: Plane-wave basis finite elements and boundary elements for three-dimensional wave scattering. Philos. Trans. R. Soc. Lond. A *362* (2004), 561–577.   Zbl 1073.78016

[16] *O. Laghrouche, P. Bettess, E. Perrey-Debain, and J. Trevelyan*: Wave interpolation finite elements for Helmholtz problems with jumps in the wave speed. Comput. Methods Appl. Mech. Eng. *194* (2005), 367–381.   Zbl pre 02167977

[17] *P. Ortiz, E. Sanchez*: An improved partition of unity finite element model for diffraction problems. Int. J. Numer. Methods Eng. *50* (2001), 2727–2740.   Zbl pre 01610504

[18] *P. Ortiz*: Finite elements using a plane-wave basis for scattering of surface water waves. Philos. Trans. R. Soc. Lond . A *362* (2004), 525–540. Zbl pre 02201054

[19] *C. Farhat, I. Harari, and L. P. Franca*: The discontinuous enrichment method. Comput. Methods Appl. Mech. Eng. *190* (2001), 6455–6479. Zbl 1002.76065

[20] *C. Farhat, I. Harari, and U. Hetmaniuk*: A discontinuous Galerkin method with Lagrange multipliers for the solution of Helmholtz problems in the mid-frequency regime. Comput. Methods Appl. Mech. Eng. *192* (2003), 1389–1419. Zbl 1027.76028

[21] *P. Rouch, P. Ladevèze*: The variational theory of complex rays: A predictive tool for medium-frequency vibrations. Comput. Methods Appl. Mech. Eng. *192* (2003), 3301–3315. Zbl 1054.74602

[22] *H. Riou, P. Ladevèze, and P. Rouch*: Extension of the variational theory of complex rays to shells for medium-freqency vibrations. J. Sound Vib. *272* (2004), 341–360.

[23] *P. Ladevèze, H. Riou*: Calculation of medium-frequency vibrations over a wide frequency range. Comput. Methods Appl. Mech. Eng. *194* (2005), 3167–3191.

[24] *I. Babuška, F. Ihlenburg, T. Strouboulis, and S. K. Gangaraj*: A posteriori error estimation for finite element solutions of Helmholtz' equation. Part I: The quality of local indicators and estimators. Int. J. Numer. Methods Eng. *40* (1997), 3443–3462. Zbl 0974.76042

[25] *I. Babuška, F. Ihlenburg, T. Strouboulis, and S. K. Gangaraj*: A posteriori error estimation for finite element solutions of Helmholtz' equation. Part II: Estimation of the pollution error. Int. J. Numer. Methods Eng. *40* (1997), 3883–3900. Zbl 0974.76043

[26] *F. Ihlenburg*: Finite Element Analysis of Acoustic Scattering. Springer-Verlag, New York, 1998. Zbl 0908.65091

[27] *I. Babuška, S. Sauter*: Is the pollution effect of the FEM avoidable for the Helmholtz equation considering high wave numbers? SIAM J. Numer. Anal. *34* (1997), 2392–2423. Zbl 0894.65050

[28] *T. Strouboulis, I. Babuška, and R. Hidajat*: The generalized finite element method for Helmholtz equation: theory, computation, and open problems. Comput. Methods Appl. Mech. Eng.. Accepted for publication.

[29] *P. J. Davis, P. Rabinowitz*: Methods of Numerical Integration. Academic Press, San Diego, 1984. Zbl 0537.65020

[30] *D. S. Jones*: Acoustic and Electromagnetic Waves. Oxford University Press, New York, 1986.

[31] *B. A. Szabó, I. Babuška*: Finite Element Analysis. John Wiley & Sons, New York, 1991. Zbl 0792.73003

[32] *T. Strouboulis, L. Zhang, D. Wang, and I. Babuška*: A posteriori error estimation for generalized finite element methods. Comput. Methods Appl. Mech. Eng. *195* (2006), 852–879.

Authors' address: *T. Strouboulis, R. Hidajat*, Dept. of Aerospace Engineering, Texas A&M University, College Station, TX 77843, U.S.A., e-mails: `strouboulis@aero.tamu.edu`, `rhidajat@tamu.edu`.